Parsing Shade

Michael O'Neal,[1] Alan R. Gillespie,[2]* Laura Gilson,[2] Van R. Kane[3]

1) Department of Geography, University of Delaware, Newark DE USA
2) Department of Earth and Space Sciences, University of Washington, Seattle WA 98195-1310 USA
3) College of Forestry Resources, University of Washington, Seattle WA USA

* Communication author: +1-206-685-8265 v, +1-206-685-2379 fax, arg3@u.washington.edu

ABSTRACT – Spectral Mixture Analysis (SMA) is a standard way of analyzing spectral images in terms of fundamental components of the scene. It accounts for lighting variations by using a *Shade* endmember that mixes with the tangible spectral endmembers such as green vegetation to produce observed spectral radiances. In forests, *Shade* comprises shadowing and topographic shading ("hillshade"), unresolved shadows cast by the canopy ("treeshade"), and shading plus shadows cast by elements of the canopy ("leafshade"). We use a 1-m LiDAR DEM to model *treeshade* over a low-relief forested area, and SMA to calculate *Shade* for an ASTER image of the same area taken near the same time of year. The differences between *treeshade* and *Shade* give remote-sensing estimates of *leafshade* in a forest dominated by deciduous trees.

Research goal – analyze image shade in a forest in terms of its unresolved constituent parts: treeshade and leafshade Λ, and make an image of Λ.

Spectral Mixture Analysis and an analytic framework

Fundamental equations

Forward linear mixing model

$$L_i = \Sigma f_j E_{i,j} + \delta_i ; \quad m < n+1 ; \quad \Sigma f_j = 1$$

- *L* — spectral radiance ($Wm^{-2}\mu m^{-1}sr^{-1}$) in image channel *i*
- *E* — *L* vector for spectral endmember *j* in image channel *i*
- *f* — fraction of endmember spectrum *E* needed to model L_i for a specific pixel
- δ — unmodeled residual for channel *i*
- *m* — number of spectral endmembers
- *n* — number of spectral image channels

Endmember spectra defined

in ASTER image DN (VNIR channels 1-3: Green, Red, NIR)

Shade (Sh)	51,	27,	30
Green Vegetation (GV)	78,	37,	134
Non-photosynthetic vegetation (NPV)	173,	146,	110

Shade endmember

$$c_0 + c_1 \cdot f_{sh} = S + (1-S) \cdot \Lambda + (1-(S+(1-S)\Lambda)) \cdot (1-a \cdot \chi(i))$$

- f_{sh} *Shade* fraction (1 = *Shade* endmember; 0 = the GV-NPV mixing line)
- c_0, c_1 calibration offset and gain factor. Image-defined endmembers may contain a fraction of shade, but f_{sh} = 0.0 should correspond to zero shade. The Shade endmember itself is defined as 100% shade.
- *S* treeshade shadow fraction, integrated to the image scale. Shadows unresolved by the LiDAR are included as a component of leafshade.
- χ integrated reflectance for the sunlit part of the canopy, For Lambertian surfaces, $\chi = 1-\cos(i)$, where *i* is the solar incidence angle; for real canopies scattering is not diffuse. For uniform reflectance, χ = 1 (this example), independent of *i*.
- *a* relative albedo, the change in f_{sh} caused by absorption of light by the surface (e.g., a leaf) relative to the albedo of tangible endmember. Albedo is a property of composition, not structure.
- Λ leafshade shadow fraction, defined shadows cast by unresolv - ed leaves and branches, integrated to the image scale. Leafshade is a property of structure, not composition.

Calibration and solution for Λ – We measured total shade f_{sh} from SMA of 15-m ASTER data and treeshade *S* using high-resolution 1-m LiDAR. Assuming *a* & Λ are constant for similar forest stands, we solved the shade endmember equation for c_1 (calibration) and f_{sh}, using two or more similar stands with different f_{sh} and *S*. c_o was -0.66; Gain c_1 was 2.58. Knowing c_0, c_1, f_{sh}, and *S*, we can solve for $a \cdot \Lambda$ for all pixels.

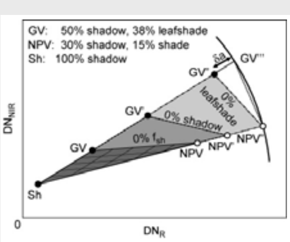

Schematic mixing diagram for the ASTER channel 3 (NIR) vs. channel 2 (R) plane. Arc is locus of a vector rotated about Sh.

The mixing plane for Sh, GV and NPV is shaded dark gray and shows isolines for f_{sh}=0 (no shade), 0.2, 0.4, 0.6, and 0.8; f_{sh}=1 (full shade) plots at Sh. Isolines for NPV (but not GV) are also shown. Shaded GV plots along the GV-Sh line; mixtures of GV and NPV plot along the f_{sh}=0 line. Mixtures with less shade than in endmembers GV and NPV (f_{sh}<0) plot beyond the f_{sh}=0 isoline.

After calibration f_{sh}, GV and NPV endmembers with no shadows plot on their respective mixing lines with Sh (GV' & NPV'). Leafshade is unchanged. Mixing now occurs in the (Sh, GV', NPV') triangle shaded intermediate gray, and the isolines for f_{sh} may be discordant with the ones in the (Sh, GV, NPV) triangle. All image data will now plot within the new triangle (no negative Sh fractions).

Extrapolation to GV'' and NPV'' gives virtual endmember positions assuming leafshade is also zero, as might occur looking down-sun. GV and NPV may have different albedoes such that vector Sh-GV'' is shorter than vector Sh-NPV: the difference is a measure of the difference in albedo δa. GV''' is the position that GV at zero phase angle would have if the albedoes were the same.

Test site -

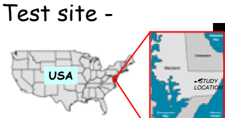

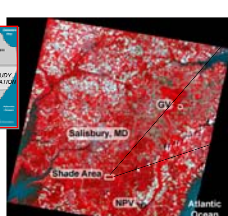

ASTER image, 15 May 2004 (60 km across; north is up). Bare fields are light; forests and wetlands are dark. Shade Area, GV, and NPV are locations used to select endmembers.

2.6 km

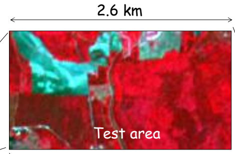

Photo of forest in eastern Maryland, figures for scale.

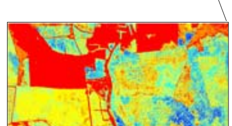

Interpretive map

Explanation

Cover classes:

Field
Red - bare earth and grass (0-1 m)
Yellow - crops, shrubs, small trees (1-5 m)

Forest – broad-leaf (hickory, oak)
orange - 5-10 m
green – 10-15 m
Light blue - 15-20 m
Blue - 20-25 m
Dark blue - 25-30 m

Air photo of test area

LiDAR images

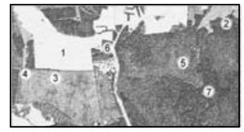

First-arrival LiDAR shade image, at full 1-m resolution and complemented so that areas of high shade are dark, as would be seen in an air photo (2.6 km across). North is up. Image shows $S+(1-S) \cdot \chi \cdot (1-a) \cdot \Lambda$.

Explanation

Numbers indicate cover classes shown in interpretive map and identified by color:

Field
1- red: bare earth and grass
2 – yellow: crops, shrubs, small trees

Forest
3 – orange: 5-10 m
4 – green: 10-15 m
5 – light blue: 15-20 m
6 – blue: 20-25 m
7 – dark blue: 25-30 m

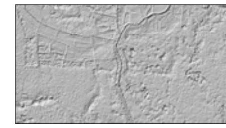

Last-arrival "bare-earth" 1-m LiDAR shade image (<9 m relief). Because test area is low-relief, hillshade could be ignored.

We extracted LiDAR images of the test area from data acquired by the State of Maryland's Department of Natural Resources between June and July of 2003. First-return point-cloud postings were <1 m, and vertical resolution was 14.3 cm.

http://dnrweb.dnr.state.md.us/gis/data/lidar/

1st-arrival 1-m LiDAR shade image embedded in 15-m ASTER image. For calculation of Λ, LiDAR images were smoothed with 15 x 15 low-pass box filters, and resampled to 15-m resolution.

S & $S \cdot \chi$ images were calculated from the 1st-arrival data using ArcInfo and ERDAS Imagine, respectively.

Results

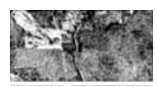

ASTER Shade fraction f_{sh} from SMA.

LiDAR shade fraction (treeshade) $S+(1-S) \cdot \chi$

LiDAR shadow fraction S

LiDAR shading fraction $\chi(i) = 1-\cos(i)$

Shade fraction images at 15-m resolutions. High-shade areas are light.

ASTER Green Veg. fraction f_{GV} from SMA

Relationship between f_{sh} and treeshade:
1) Scattergram of individual pixels
2) Four 20x20 pixel-averaged values for ASTER f_{sh} *vs.* LiDAR $S+(1-S) \cdot \chi$ *for 15-20 m stands.*

The assumption that Λ is constant appears to be valid

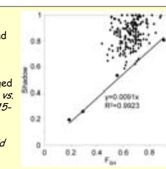

LEAFSHADE

Calculated Λ

Approximated: f_{sh}/treeshade

- Fields showed $S \approx 0$ and plants were probably not resolved. f_{sh} was dominated by *a*.
- Calibration gain $c_1 \approx 2.58$
- Assumption that Λ is constant for stands within a given age/size range is ~valid
- Permits calculation of Λ for entire image
- Λ and *S* have similar variability. Λ =0.77

a≈23%: ASTER spectral library http://speclib.jpl.nasa.gov

Discussion

Normalization of GV

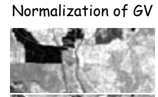

GV

$GV/(1-f_{sh})$

$GV/(1-(S-(1-S) \cdot \chi))$

- *S* is highly variable and responds to structural stage
- $(1-a) \cdot \Lambda$ appears to be less variable than S, and may prove useful in community mapping.
- The approximated version of leafshade has higher variance because it retains a component of shadow and shading. It is easier to calculate.
- *a* and Λ are not separable by this approach.
- In SMA, it is common to normalize "tangible" endmember fractions such as f_{GV} by $(1-f_{sh})$. F_{sh} includes effects due to *a* as well as Λ.
- Normalizing by LiDAR shade images, independent of *a* and Λ, produces a different result that deserves field validation and further exploration.
- Future work will take hillshade into account for rough forested terrain

Conclusions

Remotely sensed spectral images integrate the effects of lighting up to the pixel scale. Blending contributions from topography, canopies, and leaves and branches. Hybrid analysis of spectral and LiDAR images can be used to separate contributions from shadows at the tree and stand scales from shading and shadowing at sub-tree scales, and spectral mixture models can be calibrated so that spectral shade fractions (f_{sh}) correspond to more direct measurements from LiDAR. For a deciduous forest in coastal Maryland, USA, viewed in late morning during early summer, leafshade was typically ~0.5±0.1 vs. treeshade of ~0.92±0.08. Future analysis is necessary to account for topographic shading and shadowing, to incorporate a more accurate photometric function χ, and to separate darkening due to albedo *a* on a pixel-by-pixel basis.

Bibliography

Adams, J. B., and Gillespie, A. R., 2006. *Remote Sensing of Landscapes with Spectral Images: A Physical Modeling Approach.* Cambridge University Press, Cambridge, UK, 362 pp.
Adams, J. B., Smith, M. O., and Johnson, P. E., 1986, Spectral mixture modeling: a new analysis of rock and soil types at the Viking Lander I site. *Journal of Geophysical Research* 91, 8098-8112.
Dymond, J., Shepherd, J. D., and Qi, J., 2001. A simple physical model of vegetation canopy reflectance. *Remote Sensing of Environment* 75, 35 -35.
Gu, D., and Gillespie, A. R., 1998. Topographic normalization of Landsat TM images of forests based on subpixel sun-canopy-sensor geometry. *Remote Sensing of Environment* 64, 166-175.
Franklin, J., Davis, F. W., and Lefebvre, P., 1991. Thematic Mapper analysis of tree cover in semiarid woodlands using a model of canopy shadowing, *Remote Sensing of Environment* 36, 189-202.
Hall, F. G., Knapp, D. E., and Huemmrich, K. F., 1997. Physically based classification and satellite mapping of biophysical characteristics in the southern boreal forest. *Journal of Geophysical Research* 102(D24), 29,567-29,580.
Kauth, R. J., and Thomas, G. S., 1976. The tasseled cap – a graphic description of the spectral temporal development of agricultural crops as seen by Landsat. *Proceedings, Machine Processing of Remotely Sensed Data.* Purdue Univ., IN, pp. 41-51.
Li, X., Strahler, A. H., and Woodcock, C. E., 1995. A hybrid geometric optical radiative transfer approach for modeling albedo and directional reflectance of discontinuous canopies. *IEEE Transcations on Geoscience and Remote Sensing* 33, 466-480.
Retzlaff, R., Gillespie, A., Weeks, R., and Haugerud, R., 2002. Parsing the Shade Fraction of a TM Image Using Lidar Data, Kitsap County, Washington. American Society of Photogrammetry and Remote Sensing Conference, Seattle, WA, Fall.
Roberts, D.A., Adams, J.B., and Smith, M.O., 1993. Discriminating green vegetation, non-photosynthetic vegetation and soils in AVIRIS Data. *Remote Sensing of Environment* 44(2/3), 255-270.
Sabol, D. E., Jr., Gillespie, A. R., Adams, J. B., Smith, M. O., and Tucker, C. J., 2002. Structural stage in Pacific Northwest forests estimated using simple mixing models of multispectral images. *Remote Sensing of Environment* 80(1), 1-16.
Strahler, A., 1997. Vegetation canopy reflectance modeling - Recent developments and remote sensing perspectives. *Remote Sensing Reviews* 15, 179-194.
Verhoef, W., 1984. Light scattering by leaf layers with application to canopy reflectance modeling: The SAIL method. *Remote Sensing of Environment* 16, 125-141.

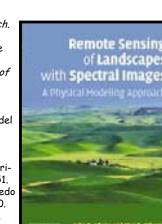

Acknowledgments

Funding to UW personnel was through OGA Contract NMO715551/1252463 and NASA Contract NNG04HZ55C (ASTER).